BIOMEDICAL ULTRASOUND IMAGING FROM 1 TO 1000 MHZ

MICHAEL KOLIOS
Department of Physics
Ryerson University, Toronto, ON, Canada

INTRODUCTION

Ultrasound refers to mechanical waves whose vibrations are above the upper limit of the human audible range (above 20 kHz). Upon recognition that ultrasound can be used in a manner similar to radar in the 1950s (in a pulse echo mode), development of ultrasound as an imaging modality followed[1,2]. In the several decades following the introduction of ultrasound, it has become one the most popular forms of imaging of the human anatomy in the world[3]. Close to 25% of all imaging procedures are based on ultrasound. The main reason is that it uses non-ionizing radiation to produce images of very good spatial resolution (in the millimeter range), is portable, relatively inexpensive and it can be used to measure function (e.g. blood flow). Most people are familiar with ultrasound imaging of the fetus, which provides detail about fetal anatomy and function. When the fetus is imaged the frequency range used is between 1 to 10 MHz, and the corresponding wavelengths are sub-millimeter. Ultrasound however is also known to also be operator dependent (in other words the operator of the ultrasound instrument can have a great effect on the quality of the image) and has, in comparison with other imaging modalities, relatively poor inherent soft tissue contrast. Therefore, many of the developments in the field of ultrasound imaging are focused on technological improvements to improve the signal to noise of the instrumentation or in the use of new techniques to increase the soft tissue contrast, such as microbubble contrast agents[4-6], elastography[7, 8], applied radiation force imaging (ARFI)[9, 10] and shear wave imaging[11, 12]. Moreover, attempts are made to make these methods quantitative, so as to avoid the operator dependence. One way to achieve this is by performing a quantitative analysis of the backscatter data prior to image formation. In this paper our attempts to study ultrasonic scattering at different length scales is presented. To achieve this, imaging at frequencies ranging from 1 MHz to 1000 MHz is performed.

ULTRASOUND IMAGING

Contrast in an ultrasound image is typically based on the strength of the backscattered ultrasound. Soft tissues adjacent to bone or air cavities strongly scatter ultrasound due to the large change in mechanical properties encountered by the pressure wave. In order to achieve good image quality and resolve small objects (such as tumors), focused transducers are used to achieve good spatial resolution in the lateral direction of the Imaging device. This focusing could be geometric (a focused transducer) or electronic (a phased array)[2]. The lateral resolution of an ultrasound imaging device depends on the frequency used and the geometrical characteristics of the focusing and is given by[13]:

$$R_{lateral} = \bar{\lambda} f_{number}$$

where $\bar{\lambda}$ is the average wavelength of the ultrasound (since usually a pulse is used for imaging) and f_{number} is the ratio of the focal length of the of the transducer to its diameter. While the equation for the lateral resolution shares many similarities with similar concepts in optics, the axial resolution is dictated by the ultrasound pulse length in time. Wide-band transducers (i.e. spanning a large frequency range or equivalently short pulses) are used to achieve greater axial resolution. The equation that describes the axial resolution of the transducer is given by:

$$R_{axial} = \frac{1}{2}\frac{c}{B}$$

where c is the speed of sound in the propagating medium and B is the bandwidth of the transducer. Increasing the transducer bandwidth increases the ultrasound spatial resolution. Therefore, higher frequencies are typically used to image smaller structures of interest to provide better axial and lateral resolution. The tradeoff, as in optics, is that the depth of field of the focused transducer decreases with greater geometrical focusing. This results in large variations in the intensity of the backscattered ultrasound in images (which his greater in the focal zone) that are a result of this focusing. The DOF can be approximated by[13]:

$$DOF = 7.0\bar{\lambda}(f_{number})^2$$

The advent of high frequency ultrasound instrumentation has made ultrasound popular beyond the clinical regime. A field in which ultrasound has grown in the last decade is that of small animal imaging (often referred to as pre-clinical imaging). For this application, typically 20-60 MHz ultrasound is used to image structures on the order of tens to hundred of microns. Typical spatial resolutions achieved are in the order of 200-30 μm lateral resolutions and 60 – 30 μm axial. This field is also termed ultrasound biomicroscopy and a comprehensive review article has been written by Foster *et al.*[13] Exquisite images of the mouse fetus have been acquired using such ultrasound imagers, clearly outlining the mouse embryo anatomy (as well as function through measurements of flow). A Canadian company based in Toronto Ontario (VisualSonics Inc. www.visulasonics.com) is currently the market pioneer and leader in this field. The increase in spatial resolution however comes at a price: that of penetration depth. For

frequencies between 20-60MHz, the imaging penetration depth is of the order of a few centimeters. At 60MHz and for a system with a dynamic range of 80dB, a tissue penetration depth of up to 6mm is expected.

In the acoustic microscopy regime the frequencies used are beyond this range (> 100 MHz).The penetration depth is limited to millimeters (100 MHz) or microns (at GHz frequencies) and therefore the applications are limited to surface measurements (such as probing tooth enamel)[14], the examination of thinly prepared specimens[15, 16] or the study of single cells[17, 18]. The same imaging considerations as stated above apply for acoustic microscopy. In this frequency range, axial and lateral resolutions of 1 μm and 3 μm can be achieved, approaching the limits of optical microscopy. One of the main advantages of acoustic compared to optical microscopy is that cells do not need to be stained and depth information can be obtained which cannot be obtained with conventional optical techniques.

ULTRASOUND SCATTERING AND TISSUE CHARACTERIZATION

While the increase in spatial resolution with frequency is straight forward and well understood, more subtle are the effects of the physics of scattering at higher frequencies, especially as the wavelength of the ultrasound approaches the size of cells, one of the most basic organizational units of tissues. Our laboratory is interested in scattering from tumors which typically have a high concentration of cells. A good understanding of the physics of scattering is required to better exploit the contrast mechanisms that ultrasound imaging can provide.

A difference in the acoustic properties of the target tissue (or the tissue structures that scatters the sound) and the acoustic properties of the background medium create the scattering of the propagating wave - which is the basis of the ultrasound signal detected (typically the backscatter). The ability to differentiate tissues based on their scattering is related to the contrast resolution of the imaging system and is an important parameter when considering various applications[2, 19]. Large contrast is achieved for example between the bone and soft tissues, as well as soft tissues and fluid filled cavities (such as cysts). When the wavelength of the ultrasound is much smaller than the structure that scatters the ultrasound, then the scattering strength can be found by using the well known equations of reflection and refraction. Assuming scattering from a plane surface between two fluid-like media with the incident wave normal to the surface, the reflected power in dB can be found:

$$dB = 10\log_{10}\frac{(Z_1 - Z_2)^2}{(Z_1 + Z_2)^2}$$

where Z_1 is the characteristic impedance of the first medium and Z_2 is the characteristic impedance of the second medium.

When the wavelength is of the order of the scatterer size, then the full equations of a traveling pressure wave incident on a structure have to be solved[20]. For high frequency ultrasound applications the ultrasound wavelengths are 20-80 μm and therefore approach the size of the typical mammalian cell. The cell shape can be approximated as spherical. The mathematical solution to a plane wave incident on a sphere exists and is given as an infinite summation. The solution is slightly simplified for fluid spheres[21] (that do not support shear waves) compared to elastic spheres[22] (that do support shear waves). Approximations however exist when the scattering structure is much smaller than the wavelength (Rayleigh scattering) or the scattering is weak (the Born approximation, an approximation that is used frequently in biomedical ultrasound)[23, 24]. These solutions typically provide the scattered pressure field as a function of the frequency of the monochromatic incident wave. An example of the solution of a pressure wave incident on a polystyrene microsphere is shown in Figure 1. This solution, even though for an elastic sphere (and therefore not fluid-like as most tissues), illustrates many important concepts in understanding scattering from biological tissues. An important parameter is the product of the wavenumber k and the scatterer size a. For low values of ka, the scattering power rapidly increases with the size of the object (or equivalently increasing frequency). This is the region of Rayleigh scattering. A transition occurs slightly above $ka = 1$, and the backscattering power does not increase substantially after this. As the frequency of the ultrasound increases above this (or equivalently the diameter of the object increases), one can indentify patterns that correspond to surface modes of the sphere[20]. Resonant scattering theory, which can solve more complex cases than a plane wave incident on a homogenous isotropic sphere, has been developed for target identification in acoustic scattering problems of greater complexity[25].

We have been able to accurately reproduce these predicted values by using high-frequency ultrasound[26]. An example is shown in figure 2. In the experiment presented a 43 μm polystyrene microsphere was suspended from a micropipette. Confocally aligned with an optical microscope was a commercial high-frequency ultrasound imager (the VEVO 770 from VisualSonics Inc., Toronto, Ontario). Scattering from the bead was recorded with a 55 MHz transducer. The red trace in the figure (left axis) corresponds to a RF (radiofrequency) line from the scattering of the bead. The blue line (right axis) corresponds to the power spectrum derived from the RF line. The complex resonances are evident both from the image and from the frequency response. Using acoustic microscopy we have recently been able to reproduce these scattering patterns using smaller diameter beads at frequencies between 100 and 1,000 MHz. For these experiments, the SASAM 1000 (Kibero GmbH, Saarbrücken, Germany) was used[27, 28]. Figure 3(A) shows C-scan and B-scan images that were generated using 200 MHz and 400 MHz ultrasound transducers from the backscatter of the polystyrene microspheres of sizes ranging

from 2 to 10 μm. As would be expected, the C-scan image generated increases in size with the increased bead diameter. The B-scan images also show the complex resonant patterns which were also seen at the 20 to 60 MHz frequency range (since the ka values are similar). Figure 3(B) shows the power spectra calculated from these backscatter patterns for different combinations of bead diameter and ultrasound frequency. Reasonable agreement is seen in our first attempts when comparing experimental data with theoretical predictions in this frequency range.

The solutions indicate that the scattered pressure variations are sensitive to the size of the scattering structures (as well as their physical attributes). This suggests the possibility of scatterer size identification in biological tissues by the examination of the frequency dependence of the scattering patterns. This has been studied extensively in the past for the clinical ultrasound frequency range[29-31] and is now being extended to higher frequency applications[32, 33]. To examine these patterns, one must have access to the raw radiofrequency data that were used to produce the ultrasound images (an example is the red trace of figure 2). These data are typically stored as voltage as a function of time (and related to space through the speed of sound) that can then can be examined as to their frequency content by their Fourier transform. Our group has extensively studied the frequency dependence of scattering as a means to identify scattering structures with an emphasis on monitoring the effects of cancer treatment and how cell scattering changes when the cells respond to treatment[26, 34-36]. It is hypothesized that since large changes in cellular structure and composition occur during cell death, the backscatter patterns would reflect these changes.

One example of how the contrast resolution changes as the frequency of the interrogating ultrasound pulse changes is that of blood scattering. In the low frequency ultrasound imaging range, blood vessels appear as black cylinders of low echogenicity as the scattering strength from the red blood cells ($ka << 1$) is very low compared to the tissue surrounding the blood vessels. However, at high frequencies ($ka \approx 1$) the scattering from the red blood cells is comparable to that of the surrounding tissue; in some cases the signal from the blood is stronger than that of the surrounding tissues. Another example is shown in figure 4. In this example, two beads are imaged with a 200 MHz transducer, one of 5 μm diameter ($ka \approx 2$) and another one of 2 μm diameter ($ka \approx 0.8$). Both beads are within the field of view of the transducer scan area. Even though the beads are of comparable sizes and have identical acoustic properties, only the 5 μm bead can be visualized with the 200 MHz transducer. The 2 μm bead cannot be detected due to its reduced scattering (roughly 25dB less, figure 1). It is hypothesized that when biological cells are imaged, an increase in the imaging frequency will introduce similar effects. When the combination of structure size and frequency of interrogation approaches $ka \approx 1$, this will result in greater contributions from those scattering structures to the overall backscatter of the biological sample. The examples mentioned in this paragraph illustrate this point. Therefore, increasing the ultrasound frequency not only improves image resolution but changes the population of scattering structures that contribute to the backscattered signal and therefore form the final image.

Due to the wave nature of ultrasound, another feature of the images produced by ultrasound is speckle. Several excellent reviews of the nature of speckle in imaging are available[37-39]. Speckle arises when there are many unresolved scatterers of similar scattering strength per resolution volume of the imaging device. In the context of ultrasonic imaging, speckle is often referred to as "speckle noise". This is because speckle can interfere with the delineation of boundaries between two media due to its "grainy" appearance. However, speckle is deterministic and for a given scattering structure the speckle pattern will remain the same. Therefore, speckle is not noise in the traditional sense. In fact, for the high frequency imaging of cells in which individual cells cannot be resolved, the entire content of the image is speckle[40]. This is seen in figure 5. Moreover, when one examines the scattering from tumors in mice, a similar speckle pattern is detected[41, 42]. Therefore the speckle pattern can relay information that is related to the scattering structures interrogated. In figure 5 a compact aggregate of acute myeloid leukemia (AML) cells is imaged. These cells have been centrifuged so as to form a tightly packed aggregate that emulates certain types of tumors in which the cell number density is very high. This aggregate was imaged at multiple frequencies: 6, 20, 40 and 200 MHz using devices that permit access to the RF data. The images generated, irrespective of the frequency used, produce a speckle pattern. This is another illustration of how the nature of the scattering structures changes as the frequency increases: the presence of speckle indicates that there are several unresolved scatterers in the resolution volume of each of the transducers used. The data presented in figure 5 suggest that at the lower frequencies, due to the large ultrasound wavelengths compared to the size of the cells (the cells are 10 μm in diameter, and the ultrasound wavelength is approximately 250 μm at 6MHz) the cell aggregate is more like a homogeneous medium and an impedance mismatch that occurs at the surface causes the specular-like reflection. However, at 40MHz, the wavelength is 37 μm which is approaching the physical size of the cell. Therefore, the surface reflection is more like diffuse scattering, and the scattering is similar in strength to that seen for further depths within the cell aggregate. This also illustrates why high frequency ultrasound is required to provide adequate sensitivity to distinguish features on the order of the cell size: it is clear that at 6MHz predominantly interfaces that enclose these cells can be distinguished rather than the signal from the cells.

CONCLUDING REMARKS

Ultrasound imaging is one of the most used imaging methods worldwide accounting for almost a quarter of all imaging procedures worldwide. In this presentation we show how the physics of scattering can influence the images

that are generated when different frequencies are used to image biological samples. Increasing the frequency of the interrogating ultrasound does not only improve spatial resolution, as would be expected from first principles, but it also changes the nature of the dominant ultrasonic scattering structures: as $ka \approx 1$ then the new structures that meet this criterion start to contribute more to the backscattered ultrasound signal detected by the transducers. Several examples presented here illustrate this principle. Our laboratory is equipped with instrumentation that allows ultrasonic interrogation with frequencies starting from 1 MHz to 1000 MHz which allows the experimental investigation of these relationships. As novel forms of imaging are developed that deal with tracers and their interactions with predominantly cellular targets (the field of molecular medicine) it is anticipated that a solid understanding of these interactions is very important for the interpretation of the ultrasound images.

ACKNOWLEDGMENTS

This research was undertaken, in part, thanks to funding from the Canada Research Chairs Program, the Canada Foundation for Innovation, the Ontario Ministry of Research and Innovation, Ryerson University and the Canadian Institutes of Health Research. The author would like to acknowledge Patrick Kennedy, Omar Falou, Eric Strohm, Dr. Min Rui, Ralph Baddour and Arthur Worthington for much of the work presented in these studies. The author would like to acknowledge the scientific input of Drs. Gregory J. Czarnota, Eric Weiss and J. Carl Kumaradas.

REFERENCES

1. R. S. C. Cobbold, *Foundations of biomedical ultrasound* (Oxford University Press, Toronto, 2007).
2. T. L. Szabo, *Diagnostic ultrasound imaging: inside out* (Elsevier/Academic Press, Boston, 2004).
3. F. Forsberg, "Ultrasonic biomedical technology; marketing versus clinical reality," Ultrasonics **42**(1), 17-27 (2003).
4. B. B. Goldberg, J. B. Liu, and F. Forsberg, "Ultrasound contrast agents: a review," Ultrasound Med Biol **20**(4), 319-333 (1994).
5. F. Forsberg, D. A. Merton, J. B. Liu, L. Needleman, and B. B. Goldberg, "Clinical applications of ultrasound contrast agents," Ultrasonics **36**(1-5), 695-701 (1998).
6. B. A. Kaufmann and J. R. Lindner, "Molecular imaging with targeted contrast ultrasound," Curr Opin Biotechnol **18**(1), 11-16 (2007).
7. J. Ophir, S. K. Alam, B. Garra, F. Kallel, E. Konofagou, T. Krouskop, and T. Varghese, "Elastography: ultrasonic estimation and imaging of the elastic properties of tissues," Proc Inst Mech Eng H **213**(3), 203-233 (1999).
8. B. S. Garra, "Imaging and estimation of tissue elasticity by ultrasound," Ultrasound Q **23**(4), 255-268 (2007).
9. J. J. Dahl, D. M. Dumont, J. D. Allen, E. M. Miller, and G. E. Trahey, "Acoustic radiation force impulse imaging for noninvasive characterization of carotid artery atherosclerotic plaques: a feasibility study," Ultrasound Med Biol **35**(5), 707-716 (2009).
10. L. Zhai, M. L. Palmeri, R. R. Bouchard, R. W. Nightingale, and K. R. Nightingale, "An integrated indenter-ARFI imaging system for tissue stiffness quantification," Ultrason Imaging **30**(2), 95-111 (2008).
11. S. Chen, M. W. Urban, C. Pislaru, R. Kinnick, Y. Zheng, A. Yao, and J. F. Greenleaf, "Shearwave dispersion ultrasound vibrometry (SDUV) for measuring tissue elasticity and viscosity," IEEE Trans Ultrason Ferroelectr Freq Control **56**(1), 55-62 (2009).
12. M. Muller, J. L. Gennisson, T. Deffieux, M. Tanter, and M. Fink, "Quantitative viscoelasticity mapping of human liver using supersonic shear imaging: preliminary in vivo feasibility study," Ultrasound Med Biol **35**(2), 219-229 (2009).
13. F. S. Foster, C. J. Pavlin, K. A. Harasiewicz, D. A. Christopher, and D. H. Turnbull, "Advances in ultrasound biomicroscopy," Ultrasound Med Biol **26**(1), 1-27 (2000).
14. S. D. Peck, J. M. Rowe, and G. A. Briggs, "Studies on sound and carious enamel with the quantitative acoustic microscope," J Dent Res **68**(2), 107-112 (1989).
15. K. Raum, "Microelastic imaging of bone," IEEE Trans Ultrason Ferroelectr Freq Control **55**(7), 1417-1431 (2008).
16. Y. Saijo, C. S. Jorgensen, P. Mondek, V. Sefranek, and W. Paaske, "Acoustic inhomogeneity of carotid arterial plaques determined by GHz frequency range acoustic microscopy," Ultrasound Med Biol **28**(7), 933-937 (2002).
17. J. Bereiter-Hahn, "Mechanics of crawling cells," Med Eng Phys **27**(9), 743-753 (2005).
18. G. A. Briggs, J. Wang, and R. Gundle, "Quantitative acoustic microscopy of individual living human cells," J Microsc **172**(Pt 1), 3-12 (1993).
19. J. F. Greenleaf and C. M. Sehgal, *Biologic System Evaluation with Ultrasound* (Springer-Verlag New York, Inc., 1992), p. 127.
20. O. Falou, J. C. Kumaradas, and M. C. Kolios, "Finite-element Modeling of Elastic Surface Modes and Scattering from Spherical Objects," in *Proceedings of the COMSOL Conference 2007*, (COMSOL, Boston, 2007).
21. V. C. Anderson, "Sound scattering from a fluid sphere," Journal of the Acoustical Society of America **22**, 426-431 (1950).
22. J. J. Faran, "Sound Scattering by Solid Cylinders and Spheres," Journal of the Acoustical Society of America **23**(4), 405-418 (1951).
23. P. M. Morse and K. U. Ingard, *Theoretical acoustics* (McGraw-Hill, New York, 1968).

24. K. S. Ratan and K. S. Subodh, "Validity of a modified Born approximation for a pulsed plane wave in acoustic scattering problems," Physics in Medicine and Biology (12), 2823 (2005).
25. L. Flax, L. R. Dragonette, and H. Uberall, "Theory of elastic resonance excitation by sound scattering," The Journal of the Acoustical Society of America **63**(3), 723-731 (1978).
26. R. E. Baddour, M. D. Sherar, J. W. Hunt, G. J. Czarnota, and M. C. Kolios, "High-frequency ultrasound scattering from microspheres and single cells," J Acoust Soc Am **117**(2), 934-943 (2005).
27. S. Brand, E. C. Weiss, R. M. Lemor, and M. C. Kolios, "High Frequency Ultrasound Tissue Characterization and Acoustic Microscopy of Intracellular Changes," Ultrasound Med Biol **34**(9), 1396-1407 (2008).
28. R. M. Lemor, E. C. Weiss, G. Pilarczyk, and P. V. Zinin, "Mechanical properties of single cells - measurement possibilities using time-resolved scanning acoustic microscopy," presented at the IEEE International Ultrasonics Symposium, 2004.
29. F. L. Lizzi, M. Astor, E. J. Feleppa, M. Shao, and A. Kalisz, "Statistical framework for ultrasonic spectral parameter imaging," Ultrasound Med Biol **23**(9), 1371-1382 (1997).
30. F. L. Lizzi, S. K. Alam, S. Mikaelian, P. Lee, and E. J. Feleppa, "On the statistics of ultrasonic spectral parameters," Ultrasound Med Biol **32**(11), 1671-1685 (2006).
31. F. L. Lizzi, M. Greenebaum, E. J. Feleppa, M. Elbaum, and D. J. Coleman, "Theoretical framework for spectrum analysis in ultrasonic tissue characterization," J Acoust Soc Am **73**(4), 1366-1373 (1983).
32. M. L. Oelze and J. F. Zachary, "Examination of cancer in mouse models using high-frequency quantitative ultrasound," Ultrasound Med Biol **32**(11), 1639-1648 (2006).
33. M. L. Oelze, W. D. O'Brien, Jr., J. P. Blue, and J. F. Zachary, "Differentiation and characterization of rat mammary fibroadenomas and 4T1 mouse carcinomas using quantitative ultrasound imaging," IEEE Trans Med Imaging **23**(6), 764-771 (2004).
34. M. C. Kolios, G. J. Czarnota, M. Lee, J. W. Hunt, and M. D. Sherar, "Ultrasonic spectral parameter characterization of apoptosis," Ultrasound Med Biol **28**(5), 589-597 (2002).
35. O. Falou, R. E. Baddour, G. Nathanael, G. J. Czarnota, J. C. Kumaradas, and M. C. Kolios, "A study of high frequency ultrasound scattering from non-nucleated biological specimens," J Acoust Soc Am **124**(5), EL278-283 (2008).
36. O. Falou, J. C. Kumaradas, and M. C. Kolios, "Finite-element modelling of acoustic wave scattering from fluid, rigid and elastic objects," Canadian Acoustics - Acoustique Canadienne **33**(3), 84-85 (2005).
37. J. W. Goodman, "Some fundamental properties of speckle," J. Opt. Soc. Am. **66**(11), 1145-1150 (1976).
38. R. F. Wagner, M. F. Insana, and S. W. Smith, "Fundamental correlation lengths of coherent speckle in medical ultrasonic images," IEEE Trans Ultrason Ferroelectr Freq Control **35**(1), 34-44 (1988).
39. S. W. Smith, G. E. Trahey, S. M. Hubbard, and R. F. Wagner, "Properties of acoustical speckle in the presence of phase aberration. Part II: Correlation lengths," Ultrason Imaging **10**(1), 29-51 (1988).
40. A. S. Tunis, G. J. Czarnota, A. Giles, M. D. Sherar, J. W. Hunt, and M. C. Kolios, "Monitoring Structural Changes in Cells with High Frequency Ultrasound Signal Statistics," Ultrasound in Medicine & Biology **31**(8), 1041-1049 (2005).
41. R. Vlad, S. Brand, A. Giles, M. C. Kolios, and G. J. Czarnota, "Quantitative Ultrasound Characterization of Responses to Radiotherapy in Cancer Mouse Models," Clinical Cancer Research **15**(6), in press (2009).
42. R. M. Vlad, N. M. Alajez, A. Giles, M. C. Kolios, and G. J. Czarnota, "Quantitative ultrasound characterization of cancer radiotherapy effects in vitro," Int J Radiat Oncol Biol Phys **72**(4), 1236-1243 (2008).

FIGURES

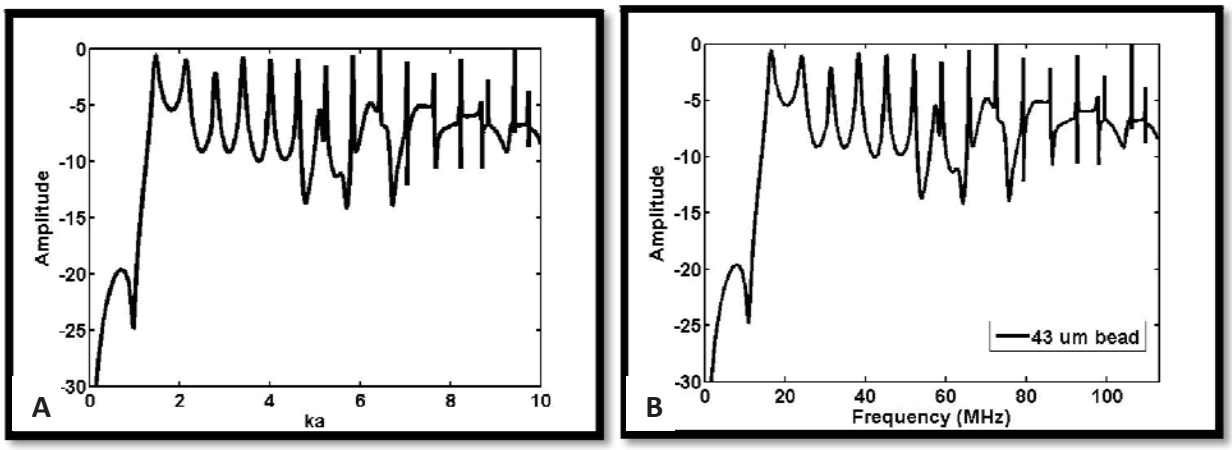

Figure 1: The Faran solution to scattering of a plane wave incident on an elastic, isotropic and homogeneous sphere. A) Normalized backscatter power (to the maximum value) is plotted as a function of the wave number times the sphere diameter (ka). B) Normalized backscatter power plotted as a function of ultrasound frequency for a given scatterer size (a = 43 µm) for the same parameters in (A).

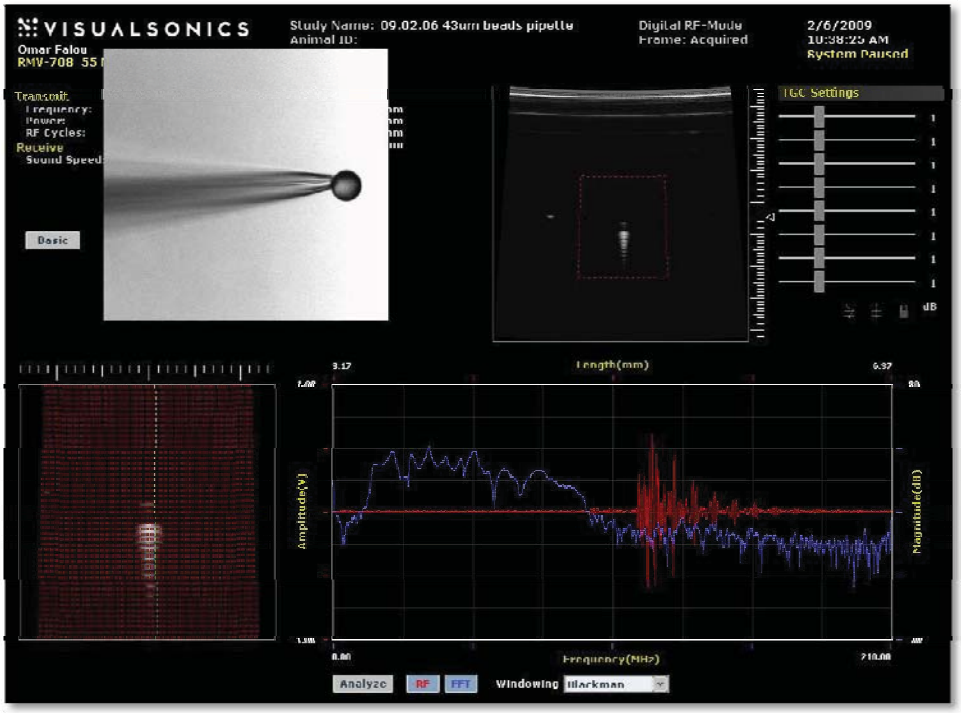

Figure 2: Single bead scattering measured using a high-frequency ultrasound system (the VEVO 770 using a 55MHz transducer in this experiment). In the top left corner of the image an optical microscopy image of a 43 µm polystyrene microsphere that is held in position by a micropipette and confocally aligned with the transducer). To the right of this picture the B-mode ultrasound image of the bead (seen closer up in the bottom left). The resonant pattern is clearly seen. In the bottom right of the image the red line represents a single radiofrequency trace of the scattered ultrasound and the blue line represents power spectrum derived from this a line. The resonant patterns of figure 1(B) can be seen in the power spectrum.

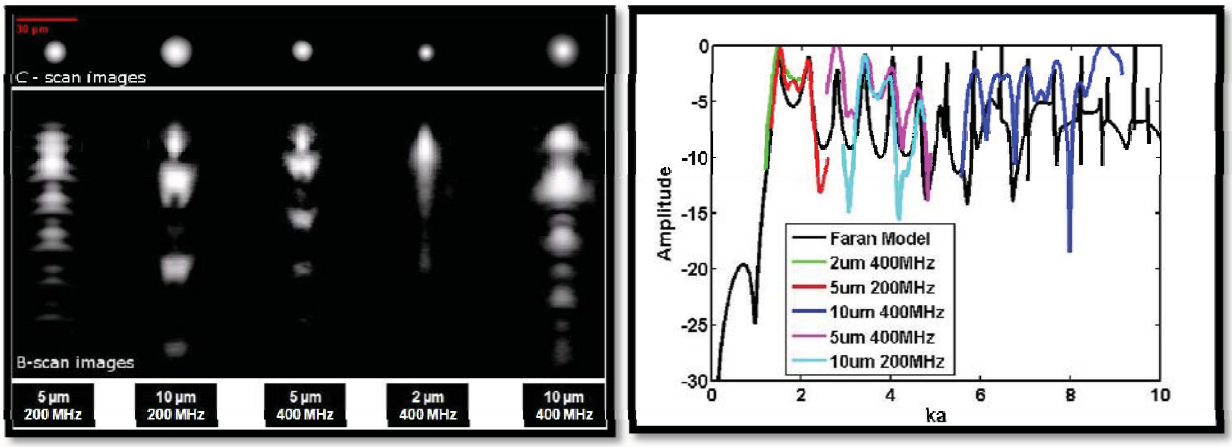

Figure 3: Bead scattering using acoustic microscopy. A) C-scan (top) and B-scan images shown for 5 combinations of bead size (2-10 □m) and interrogation frequency (200 or 400MHz). C-scans illustrate full-with half maximums of spheres of similar size to actual bead dimensions, and B-scans with characteristic resonant patterns. B) Power spectra of the various combinations of frequencies and transducers superimposed on the Faran solution for scattering, showing good agreement at locations of the peaks in the backscatter power spectrum.

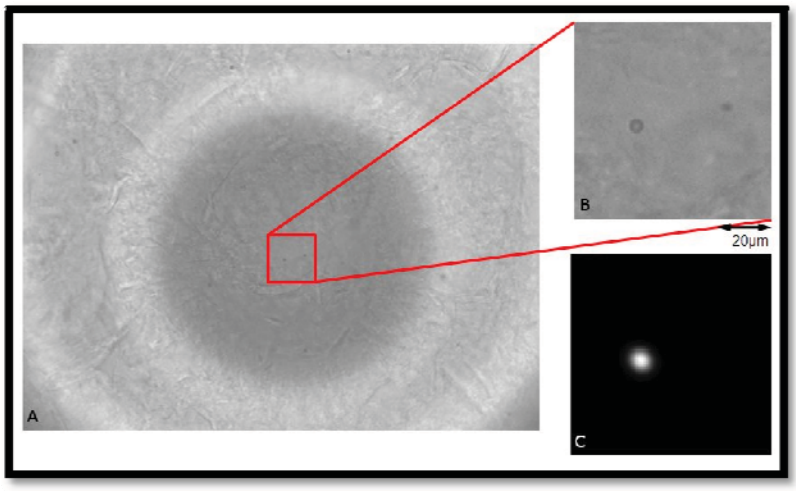

Figure 4: Demonstration of the effect of ultrasound contrast resolution. The above image was taken using the Kibero SASAM 1000 acoustic microscope that confocally aligns and optical microscope with the acoustic transducer (200MHz used in this example). A) Optical microscopy image of the specimen imaged with the acoustic microscope. The circle in this image represents the transducer cavity as seen from the optical microscope underneath. The region enclosed in the red square was scanned with the acoustic microscope. B) a zoom of the region scanned shows to polystyrene microspheres in the region, one of 5 µm diameter (to the left) and one of 2 µm diameter (to the right). C) The acoustic microscopy image clearly shows the 5 µm bead but detects no signal from the area the 2 µm bead is located. This could be understood by inspection of figure 1: the scattering from the smaller bead is much weaker.

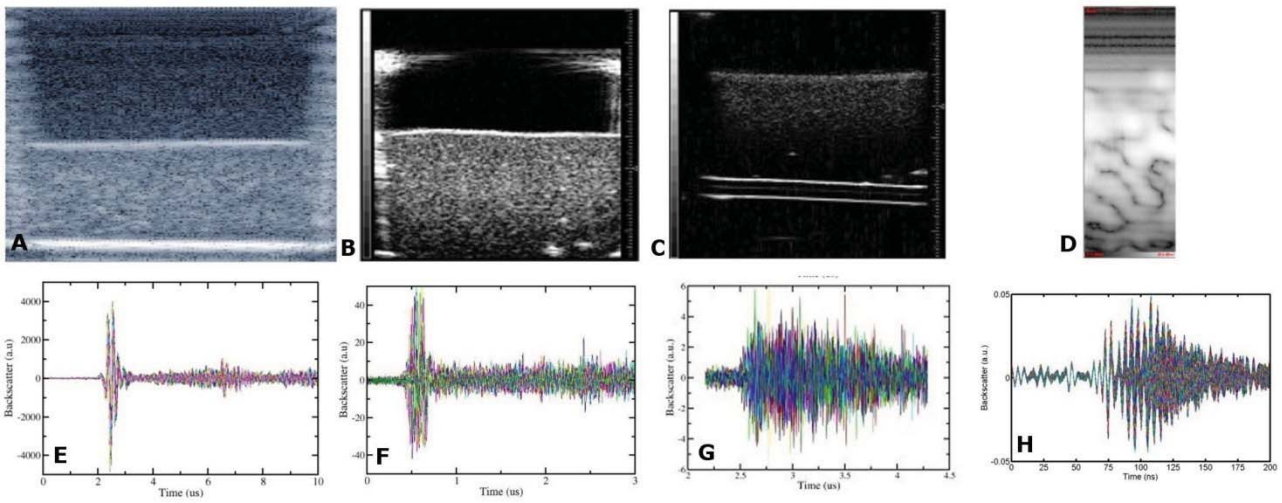

Figure 5: B scan images (top row) and a superimposed collection of RF lines that formed the images (bottom row) from a compact aggregate of acute myeloid leukemia cells. The aggregate has a height ranging from 1-10mm. The data were collected at 6MHz (with an Ultrasonix RP instrument, panels A,E), 20MHz (B,F with a VisualSonics VEVO 770 instrument, 8mmX8mm), 40MHz (C,G with a VisualSonics VEVO 770 instrument, 8mmX8mm) and 200MHz (D,H with a Kibero SASAM 1000 instrument). Image scale varies in each panel. Assuming the cell as the dominant scattering source, this represents a large range in ka .In all cases a speckle pattern is detected. At the lower frequencies, scattering from the aggregate surface dominates while at higher frequencies scattering from the cells dominates.

In a Class *of its Own*

The unmistakable look of Hand-held Analyzer Type 2270 can overshadow a number of discrete yet significant distinctions which make this powerful instrument the complete toolbox for sound and vibration professionals. These include:

- Integrated digital camera
- Two-channel measurement capability
- Integrated LAN and USB interfaces for fast data transfer to PC and remote control and monitoring of Type 2270
- Environmental protection IP44

Versatile in the Extreme

Type 2270 also boasts a wide range of application software modules that can be licensed separately so you get what you need when you need it.

Currently available measurement software includes:

- Sound Level Meter application
- Real-time frequency analysis
- Logging (noise level profiling)
- Sound and vibration recording
- Building acoustics
- Tonal assessment

Type 2270 meets the demands of today's wide-ranging sound and vibration measurement tasks with the accuracy and reliability associated with Brüel & Kjær instrumentation.

To experience the ease-of-use of Type 2270, just go to www.bksv.com and view the on-line video demonstrations.

For more information please contact your local Brüel & Kjær representative

HEADQUARTERS: DK-2850 Nærum · Denmark · Telephone: +4545800500
Fax: +4545801405 · www.bksv.com · info@bksv.com

Australia (+61)29889-8888 · Austria (+43)18657400 · Brazil (+55)115188-8166
Canada (+1)514695-8225 · China (+86)1068029906 · Czech Republic (+420)267021100
Finland (+358)9-755950 · France (+33)169907100 · Germany(+49)42117870
Hong Kong (+852)25487486 · Hungary (+36)12158305 · Ireland (+353)18037600
Italy (+39)025768061 · Japan (+81)337798671 · Republic of Korea (+82)234730605
Netherlands (+31)318 55 9290 · Norway (+47)66771155 · Poland (+48)228167556
Portugal (+351)214711453 · Singapore (+65)3774512 · Slovak Republic (+421)254430701
Spain (+34)916590820 · Sweden (+46)84498600 · Switzerland (+41)18807035
Taiwan (+886)227139303 · United Kingdom (+44)1438739000 · USA (+1)8003322040

Local representatives and service organisations worldwide

Hand-held Analyzer *Type 2270*

Brüel & Kjær